Chapter 13
Time-Resolved Spectroscopy of NAD(P)H in Live Cardiac Myocytes

Alzbeta Marcek Chorvatova

Abstract Monitoring cell and tissue physiological parameters, such as metabolic state in real time and in their true environment is a continuous challenge. In the last decades, advanced photonics techniques were developed, combining fluorescence spectroscopy with time-resolved and imaging techniques, thus opening completely new opportunities for investigation of fluorescence parameters in living cells. This is particularly true in the case of evaluation of endogenous fluorescence or autofluorescence (AF) of living cells, derived from nicotinamide dinucleotide (phosphate) (NAD(P)H). We have pioneered the application of time-resolved fluorescence spectroscopy to evaluate changes in metabolic oxidative state directly in living cardiac cells by means of endogenous NAD(P)H fluorescence. NAD(P)H fingerprinting was investigated in living cardiac myocytes isolated from left ventricle (LV) of rats by spectrally-resolved lifetime detection using spectrally-resolved time-correlated single photon counting (TCSPC). Metabolic modulation was employed to evaluate individual NAD(P)H fluorescence components. Advanced data analysis leading to development of techniques and analytical approaches aimed at precise separation of individual fluorescence components from the recorded AF signals was also performed. Spectral decomposition of time-resolved NAD(P)H fluorescence signals by linear unmixing approach was successfully achieved. Gathered results demonstrate that combined approaches between time-resolved, spectroscopic and imaging systems open new possibilities for understanding the precise role of mitochondria in complex pathophysiological conditions and for finding new non-invasive clinically-relevant diagnostic applications.

A. Marcek Chorvatova (✉)
Department of Biophotonics, International Laser Centre, Bratislava, Slovakia
e-mail: alzbeta.chorvatova@ilc.sk

W. Becker (ed.), *Advanced Time-Correlated Single Photon Counting Applications*,
Springer Series in Chemical Physics 111, DOI 10.1007/978-3-319-14929-5_13

13.1 Non-invasive Investigation of Metabolic Oxidative State in Living Cardiac Myocytes

Metabolism is crucial for cardiac cell contraction. The heart is a pump converting chemical energy into mechanical work and the power for this work is gathered almost entirely from oxidation of carbon fuels and, to a great extent, these fuels are provided by coronary (myocardial) blood flow. In the heart, oxidative metabolism is primarily the function of mitochondria in the process of oxidative phosphorylation by the respiratory chain [17]. This process is coupled with the oxidation of NADH, the principal electron donor for the electrochemical gradient that is indispensable for oxidative energy metabolism. The first step in this process, which accounts for 95 % of ATP generation needed for cardiomyocyte contraction, is the dehydrogenation of NADH by flavoproteins of Complex I of the mitochondrial respiratory chain. Because of the high oxidative metabolism, heart cells have enhanced oxidative capacity, demonstrated by their ultrastructure [4]: 25–35 % of total cardiomyocyte volume is occupied by mitochondria, distributed in stripes, where oxidative phosphorylation takes place. Energy generated by the network of cardiac cells serves for the main function of the heart—its contraction—allowing the pumping of the blood. Mitochondrial role in cellular bioenergetics predestine them to play a pivotal role in various human diseases—the implication of the mitochondrial dysfunction in CV disease was largely reviewed [2]. Possibility to study, non-invasively, rapid changes in metabolic oxidative state is therefore crucial for understanding of processes in living cardiac cells and their alterations in pathophysiological conditions.

In the CVS, endogenous fluorescence of NAD(P)H and flavins has long been used for non-invasive monitoring of processes, such as modifications in metabolic oxidative state, or change in myocardial tissue status (reviewed in [28]). Dehydrogenation of NADH, the principal electron donor for the electrochemical gradient, by flavoproteins of the mitochondrial respiratory chain is indispensable for ATP generation and thus oxidative energy metabolism. In addition, during oxidative stress, cellular NADPH content is modulated through the release of peroxides and various by-products that have been shown to decrease the activity of several enzymes, such as NADP-isocitrate dehydrogenase. In the last decades, advanced photonics techniques have been developed to monitor endogenous fluorescence in living cells and tissues [25, 30].

13.1.1 Experimental Set-up for Time-Resolved NAD(P)H Recordings on Living Cardiac Cells

The experimental setup is shown in Fig. 13.1 It consists of a Zeiss Axiovert 200 microscope, a Becker & Hickl 375 nm picosecond diode laser, a Proscan Solar 100 spectrograph, and a PML-16 multichannel detector and an SPC-830 TCSPC module from Becker & Hickl.

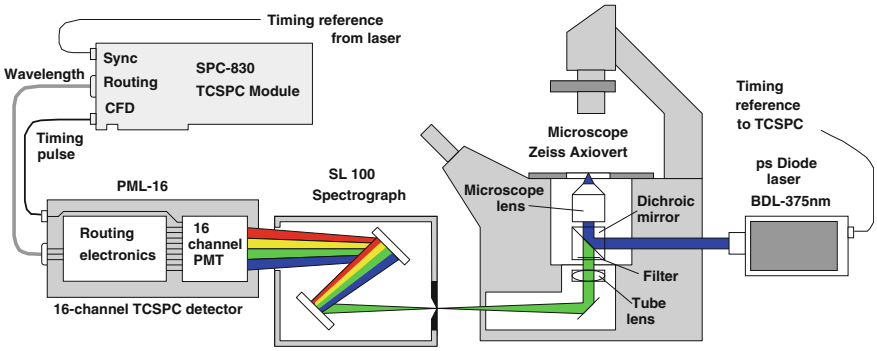

Fig. 13.1 Experimental setup for time-resolved fluorescence spectroscopy. A 375-nm picosecond laser diode (Becker & Hickl) was used as an excitation source with ~1 mW output power. The emitted cell autofluorescence, separated from laser excitation by 395 nm dichroic and 397 nm long-pass filter in the Axiovert 200 M (Zeiss, Canada), was spectrally dispersed by an imaging spectrograph (Solar SL 100 M, Proscan, Germany), detected by a PML 16 16-channel TCSPC detector and recorded by an SPC-830 TCSPC module, both Becker & Hickl, Germany. Described in detail in [20]

The collimated beam of the picosecond diode laser is sent through the back port of the microscope. There it is reflected by a dichroic mirror in a standard beamsplitter cube in the filter carousel of the microscope, and focused into the sample by the microscope lens. It creates a slightly defocused elliptical spot with typical dimensions of 10 × 20 μm, chosen in regard to average the fluorescence signal over the width of a single myocyte [4]), see inset in Figs. 13.4, 13.7.

The fluorescence is detected back through the microscope lens, and separated from the excitation light by the dichroic mirror in the filter cube. A filter at the output of the filter cube suppresses scattered excitation light. The tube lens of the microscope focuses the light from the illuminated area into the output image plane at the side port of the microscope.

The spectrograph is put into this plane with its input slit. The spectrograph projects a spectrum of the fluorescence signal on the cathode of an R5099-L16 16-channel PMT inside the PML-16 detector module. The detector module contains routing electronics which provides, for every photon detected, a timing pulse and a routing signal. The routing signal indicates the PMT channel in which the photon was detected. The timing pulse and the routing signal are fed into the SPC-830 TCSPC module which builds up a photon distribution over the times of the photons after the laser pulses and the detector channel, see Chap. 1, Sect. 1.4.1 for details. The result is a 2-dimensional data array that contains individual decay curves for the 16 wavelengths. Because the decay curves are built up simultaneously, motion in the cardiomyocytes or photobleaching do not cause distortion in the recorded spectra. The setup and its application to the study of cardiac myocytes are described in [20, 29, 31].

For the results presented here, fluorescence decays were measured for 30 s in the 16 spectral channels simultaneously over a wavelength range of 385–675 nm.

The half-width of the instrument response function (IRF) was estimated to be 0.2 ns [20] with the temporal resolution of the system set to 24.4 ps/channel. Cells were mounted on an inverted microscope and studied at room temperature in 4-well chambers with UV-proof, coverslip-based slides (LabTech, Canada). Data were always evaluated from the first measurement of each cell (measured for 30 s) to avoid artefacts induced by photobleaching.

13.1.2 Time-Resolved Fluorescence Spectroscopy of NAD(P)H in Vitro

Measurement of the fluorescence of endogenous fluorophores in vitro is a prerequisite for demonstrating their presence in living cells, as well as for having reference spectra for separation of individual components. NADH and NADPH are endogenously fluorescent molecules [30]; their fluorescence spectra and fluorescence lifetimes (Fig. 13.2A) were studied in vitro in the intracellular media-mimicking solution (pH 7.25) [1, 29]. Spectral intensity was linearly dependent on the NADPH concentration (Fig. 13.2Aa), as illustrated at the maximum emission wavelength of 450 nm (Fig. 13.2Ac) with no modification in the fluorescence decays

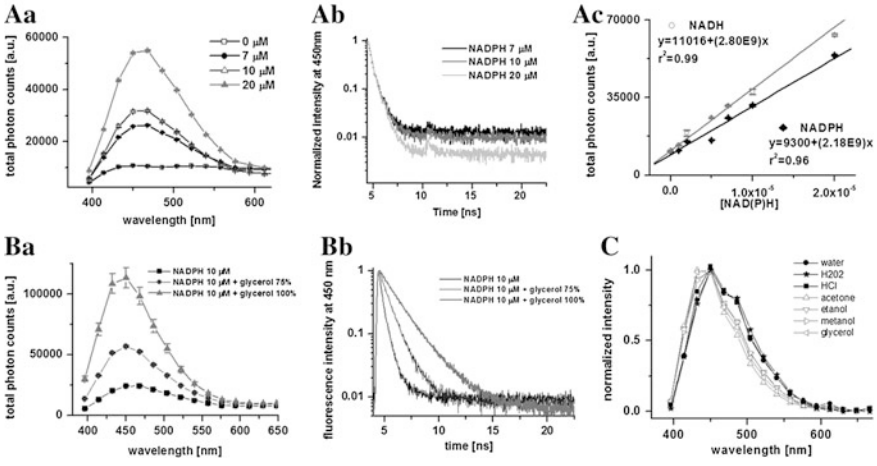

Fig. 13.2 NAD(P)H fluorescence in vitro. **A** Concentration-dependence of NADPH fluorescence in the intracellular media-mimicking solution (pH 7.25), excitation 375 nm. Background-corrected emission spectra (**a**), normalized fluorescence decays at 450 nm (**b**) and the total photon counts at 450 nm (**c**) as a function of the NADH and NADPH concentration. **B** Viscosity-dependence of the NADPH (10 μM) fluorescence in intracellular solution. Background-corrected emission spectra (**a**) and normalized fluorescence decays at 450 nm (**b**). Data are shown as mean ± SEM (n = 5 for all but 0 μM for which n = 3). **C** Normalized spectra of NADH (20 μM) in inorganic (*grey*) and organic (*black*) solvents (all 100 %). Published in [1, 29]

(Fig. 13.2Ab). Normalized spectra for NADPH concentrations from 1 to 20 μM overlaid perfectly (data not shown), confirming the same molecular origin. Comparable results were obtained for NADH, in accordance with the fact that NADH and NADPH are inseparable by fluorescence spectra, or fluorescence lifetimes, only with slightly higher quantum yield for NADH than for NADPH (Fig. 13.2Ac) [1, 89].

To test the sensitivity to molecular environment, we have recorded NADH and NADPH in different organic and inorganic solvents (Fig. 13.2B and C). As illustrated by the addition of different concentrations of glycerol versus H_2O, the total photon counts, measured at the emission maximum (λ_{em} = 450 nm) revealed exponential rise of the peak of NADPH fluorescence intensity (Fig. 13.2Ba) [29]. This result was due to the prolongation of the fluorescence lifetimes in a highly viscous environment (Fig. 13.2Bb) and is in agreement with previous findings [46] showing that the sensitivity of NADPH fluorescence intensity to changes in its microenvironment can be related to changes in the molecular mobility and/or modification in the conformation of NADPH molecules in more viscous milieu. Importantly, we also noted a slight (10 nm) blue spectral shift when NADH or NADPH fluorescence was recorded in organic solvents, as opposed to the inorganic ones (Fig. 13.2C). These experiments also demonstrated sensitivity of the constructed experimental set-up for recording physiological concentrations of these endogenous fluorophores.

13.1.3 Time-Resolved NAD(P)H Fluorescence Spectroscopy in Cardiac Mitochondria

Cardiac mitochondria are crucial for the heart oxidative metabolic status, as they contain respiratory chain responsible for the ATP production in cardiac cells. To demonstrate that, in cardiomyocytes, the presence of endogenous fluorescence derived from NAD(P)H primarily related to these organelles, confocal images of unstained myocytes were gathered by the 2 photon excitation induced by 777 nm light to verify NAD(P)H fluorescence distribution (Fig. 13.3a). Recorded images clearly demonstrated that endogenous NAD(P)H fluorescence in cells was distributed in stripes.Verification of mitochondrial distribution using mitochondrial fluorescence probe Tetramethylrhodamine (TMRM) confirmed stripe-like distribution of mitochondria [4]. These results are in agreement with 2 photon microscopy and spectroscopy recording used previously to evaluate spatial distribution and intensity changes of NAD(P)H fluorescence in living cardiac myocytes [59]. AF excitation-emission spectra in heart mitochondria isolated from rat hearts by differential centrifugation [23] demonstrated presence of both NAD(P)H and flavin fluorescence (Fig. 13.3b). This result revealed comparable peaks to those recorded in cardiac myocytes [23] and was also in agreement with previous observations in pigeon heart mitochondria that identified excitation/emission spectra of oxidized

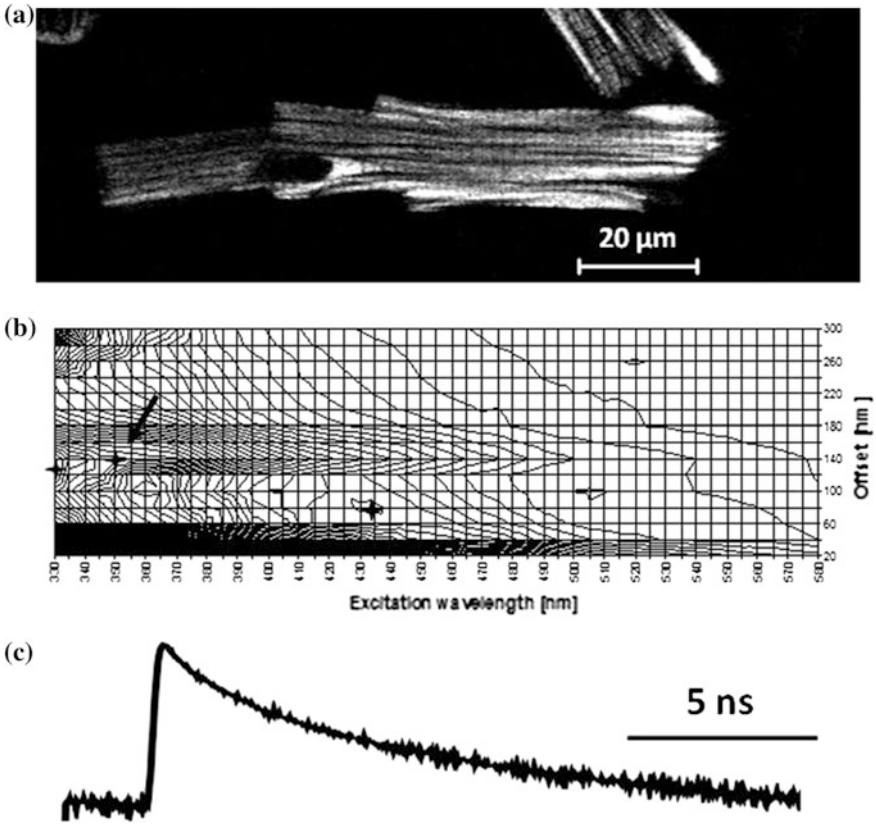

Fig. 13.3 Mitochondrial NAD(P)H fluorescence of rat cardiac cells. **a** Confocal image of NAD(P)H distribution in a cardiac cell (777 nm two-photon excitation, HFT KP 700/488 dichroic filter and 450–470 nm spectral range for emission detection). **b** Excitation-emission matrix recorded in isolated cardiac mitochondria (*arrow* points to the NAD(P)H peak) by spectro-fluorimetry. **c** Example of the NAD(P)H fluorescence decay recorded in isolated rat cardiac mitochondria after excitation by 375 nm laser by time-resolved fluorescence. For more details, see [23, 58]

flavoproteins and reduced pyridine nucleotide fluorescence [16]. Time-resolved measurements from isolated mitochondria after excitation at 375 nm showed at least a double exponential decay of 0.47 and 1.32 ns (Fig. 13.3c) [58]. These results correspond to data in intact porcine heart mitochondria, where 3 NAD(P)H fluorescence lifetime pools have been identified [10]: a free pool with a lifetime of 0.2–0.4 ns, an intermediate pool (1–2 ns), and a long lifetime pool (3–8 ns). The intermediate and long lifetime pools were proposed to be resulting from protein binding of NAD(P)H.

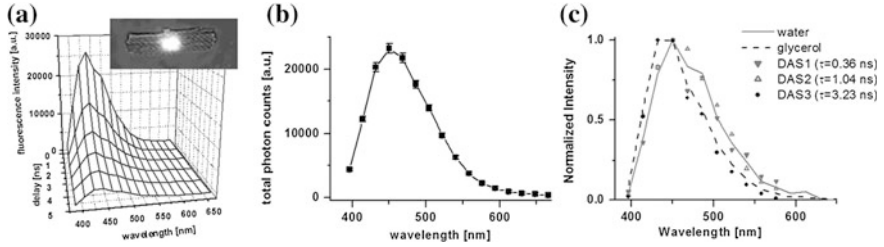

Fig. 13.4 Spectrally- and time-resolved AF of cardiac myocytes. **a** Original recording of the time-resolved spectroscopy measurements of NAD(P)H fluorescence in living cardiac cells, excitation at 375 nm (mean of 10 measurements; in the inset, representative transmission image of the single cardiomyocyte illumination). **b** Total photon counts of NAD(P)H fluorescence in rat cardiac myocytes in control conditions (Data are shown as mean ± SEM, n = 70 cells). **c** Decay associate spectra for estimated fluorescence lifetimes. Published in [20, 33, 39]

13.1.4 Time-Resolved NAD(P)H Fluorescence Spectroscopy in Isolated Cardiac Myocytes

Recording of time- and spectrally-resolved fluorescence from isolated living LV cardiomyocytes was highly reproducible for both NAD(P)H (Fig. 13.4a) [21, 29, 31] and flavins [23, 24]. Cardiac myocytes were isolated from LV of female rats after retrograde perfusion of the heart with proteolytic enzymes, as previously reported [5, 32]. Steady-state emission spectra of the cardiomyocyte NAD(P)H fluorescence, calculated from the total photon counts on each spectral channel, had a spectral maximum at 450 nm (Fig. 13.4b). Analysis of the AF decay recorded in cardiomyocytes showed acceptable chi-square values ($\chi^2 < 1.2$) and flat plots of weighted residuals when using at least a 3-exponential model with lifetimes (Table 13.1). Gathered data are in good agreement with lifetime values estimated in cardiomyocyte mitochondria [10], as well as in human cardiac myocytes [18, 19].

13.2 Analysis of Individual NAD(P)H Fluorescence Components

Finding an appropriate analytical approach for analysis of time-resolved fluorescence data, particularly when performed in living cells and tissues, is a prerequisite to insure that physiological significance of the recorded data is correctly recovered [64]. At the same time, it is also one of the main limitation of fluorescence lifetime imaging (FLIM) recordings, in regard to large amount of complex data, as well as in regard to availability of the sufficient number of photons for each measurement point. The physically relevant models need to include the general knowledge of the investigated system, together with the established statistical properties of the residuals [82].

Table 13.1 Fluorescence parameters of cardiomyocyte AF ($\lambda_{excitation/emission}$ = 375 nm/450 nm)

	Photon counts (a.u.)	a_1	τ_1 (ps)	a_2	τ_2 (ps)	a_3	τ_3 (ps)	χ^2
Control (70/13)	23231 ± 786	69.29 ± 1.04	685.68 ± 10.80	27.63 ± 0.92	2028.23 ± 52.09	3.14 ± 0.23	12678.87 ± 776.84	1.02 ± 0.01
Rotenone (28/6)	58940 ± 1833*	71.04 ± 1.63	563.92 ± 10.28^{*+}	26.25 ± 1.48	1696.32 ± 56.78*	2.95 ± 0.22^{+}	8757.18 ± 649.78	1.05 ± 0.01
Cyanide (10/2)	55384 ± 7002*	68.80 ± 1.33	485.71 ± 12.62^{*+}	28.80 ± 1.21	1582.34 ± 55.32^{*+}	2.47 ± 0.18^{+}	9431.74 ± 1274.96	1.01 ± 0.01
Rotenone/cyanide (10/2)	55603 ± 3556*	72.3 ± 1.80	555.54 ± 16.42	25.00 ± 1.56	1688.47 ± 91.04	2.71 ± 0.34	8481.59 ± 701.50	1.05 ± 0.02
DNP (15/3)	10824 ± 990$^{*\#}$	67.29 ± 1.65	901.42 ± 54.61$^{*\#}$	27.07 ± 1.72	2162.46 ± 118.57$^{\#}$	5.59 ± 0.80$^{*\#}$	15828.98 ± 1828.51$^{\#}$	1.01 ± 0.01
BHB/AcAc (20:1) (27/4)	29308 ± 1553$^{*\&}$	66.3 ± 1.64	598.31 ± 22.38	31.05 ± 1.50	1801.64 ± 64.66	2.78 ± 0.26	12597.52 ± 1427.89	1.01 ± 0.01
BHB/AcAc (2:1) (26/4)	21544 ± 1099	64.96 ± 1.99	657.52 ± 21.66	31.38 ± 1.92	1855.63 ± 65.37	3.72 ± 0.25	10848.68 ± 683.22	1.00 ± 0.00
Lactate/pyruvate (15/3)	24066 ± 1861	65.73 ± 2.66	655.47 ± 23.61	30.87 ± 2.32	1893.02 ± 117.35	3.63 ± 0.47	10380.86 ± 2009.34	1.01 ± 0.00

	P_{max} (a.u.)	$a_1\tau_1$ (a.u.) ($^{*}10^3$)	r_1	$a_2\tau_2$ (a.u.) ($^{*}10^3$)	r_2	$a_3\tau_3$ (a.u.) ($^{*}10^3$)	r_3	$<\tau>$ (ns)
Control (70/13)	1546 ± 68	48.00 ± 1.26	0.36 ± 0.01	53.57 ± 1.00	0.40 ± 0.01	32.69 ± 1.71	0.24 ± 0.01	1.34 ± 0.03
Rotenone (28/6)	3565 ± 160*	40.46 ± 1.53	0.36 ± 0.02	42.54 ± 0.96^{*+}	0.40 ± 0.01	23.13 ± 1.1.05	0.22 ± 0.01	1.06 ± 0.01*
Cyanide (10/2)	3638 ± 468*	33.54 ± 1.42*	0.33 ± 0.01	45.16 ± 1.31	0.45 ± 0.01	21.65 ± 1.00^{+}	0.22 ± 0.01	1.00 ± 0.02*
Rotenone/cyanide (10/2)	3762 ± 230*	40.42 ± 2.09	0.39 ± 0.02	40.99 ± 0.72*	0.40 ± 0.01	21.19 ± 1.38	0.21 ± 0.02	1.03 ± 0.01*
DNP (15/3)	771 ± 95$^{*\#}$	60.51 ± 3.69$^{*\#}$	0.32 ± 0.02	59.12 ± 5.21$^{\#}$	0.31 ± 0.02$^{*\#}$	74.62 ± 7.20$^{*\#}$	0.38 ± 0.02$^{*\#}$	1.94 ± 0.12$^{*\#}$
BHB/AcAc (20:1) (27/4)	1982 ± 95$^{\$}$	40.06 ± 2.20	0.32 ± 0.02	54.38 ± 1.31	0.44 ± 0.01	30.06 ± 1.22	0.24 ± 0.01	1.24 ± 0.02
BHB/AcAc (2:1) (26/4)	1386 ± 74	43.62 ± 2.56	0.32 ± 0.02	55.71 ± 2.10	0.41 ± 0.02	37.46 ± 1.76	0.27 ± 0.01	1.37 ± 0.02
Lactate/pyruvate (15/3)	1480 ± 93	43.75 ± 2.95	0.34 ± 0.02	55.19 ± 1.54	0.43 ± 0.01	30.54 ± 2.68	0.23 ± 0.02	1.29 ± 0.02

Total photon counts, fluorescence lifetimes (τ_1–τ_3) and their relative amplitudes (a_1–a_3) of single cardiomyocytes in control conditions and in the presence of 1 μmol/L rotenone, 4 mmol/L cyanide, 50 μmol/L DNP, 3 mmol/L BHB with 150 or 1.5 mmol/L AcAc (ratio 20:1 and 2:1, respectively), lactate (1 mmol/L) in the presence of pyruvate (100 μmol/L) or octanoate (1 mmol/L). In grey, maximum AF emission (P_{max}; time-resolved at Δt = 0 ns), calculated relative intensities and relative fractions for each component as well as average lifetime. Data are shown as mean ± SEM (number of cells/number of animals); $^{*}p < 0.05$ versus control, $^{\#}p < 0.05$ versus rotenone, $^{\&}p < 0.05$ versus BHB/AcAc (ratio 2:1).

The separation and quantification of individual components underlying multi-exponential decays of autofluorescing species in biological cells and tissues still represent tough scientific challenges that have not yet been fully resolved. Searching for the best approach for precise separation of fluorescence from individual fluorophores directly in living cells and tissues is therefore one of the main tasks to solve.

13.2.1 Global Analysis and Decay Associated Spectra (DAS)

Typical approach to analyze fluorescence decay (illustrated in Fig. 13.3c) is to fit the decay curve, while establishing discrete components—fluorescence lifetimes—for each fluorescence decay. This approach allows to calculate relative intensities and relative fractions for each component, as well as an average fluorescence lifetime for each decay (Table 13.1). However, although this approach can serve to distinguish between distinct cellular states, it has several limitations. On one hand, such components do not necessarily match the fluorescence lifetime distribution for such system. On the other hand, values thus gathered cannot easily be related to one precise fluorescence component. One solution is to estimate spectral shapes of underlying components by recording the fluorescence decays on multiple wavelengths (Fig. 13.4a), which is useful to link lifetimes with variable amplitudes. In such case, spectral coordinates can be processed to create a set of decay-associated spectra (DAS), corresponding to individually-resolved lifetimes, estimated by global analysis [61, 88]. The DAS for cardiomyocyte NAD(P)H fluorescence (Fig. 13.4c) were constructed for each lifetime pool as a product of wavelength-dependent fractions of the NAD(P)H fluorescence emission of each lifetime pool with respect to total fluorescence, multiplied by total photon counts [10]. The resulting DAS showed that, for cardiomyocytes in control conditions, the 1st and 2nd lifetime pools with sub-nanosecond decay kinetics had similar spectra with maximum around 450–470 nm and red-shifted shoulder at 490 nm, while the 3rd lifetime pool with the longest lifetime has a blue-shifted peak with the maximum around 430–450 nm. Comparison of the first two spectra observable in the cells to the spectral profiles of NADH showed almost perfect fit of the component measured in water (and in inorganic solvents in vitro, Fig. 13.2c, in general), with the first two DAS components, as well as a very good fit of the glycerol- (and organic solvents in general)-like component to the third DAS component. These results uncover the presence of two spectrally-distinct components in UV-excited AF of cardiac cells with 3 fluorescent lifetimes. However, although this result gives an indication of underlying fluorescence species and their spectral shapes, it is of a limited use in complex cellular environment.

13.2.2 Time-Resolved (TRES) and Area-Normalized (TRANES) Emission Spectra

To estimate the number of individual spectral components present in the fluorescence decays recorded in complex environment of living cardiac cells, an approach proposed for semi-quantitative analysis of the multi-fluorophore mixtures [62] was applied. Series of consecutive spectral profiles decaying in time, time-resolved emission spectra (TRES) sequences were computed from original multi-wavelength TCSPC recordings of NAD(P)H fluorescence by summing the data in several consecutive temporal windows (Fig. 13.5a), as previously described for flavin fluorescence [20]. TRES analysis offers an alternative approach to DAS by estimating spectral components in complex sample. In addition, TRANES—area normalized TRES—method [62] where the spectra are further background subtracted and normalized, indicates the number of the most pronounced fluorescence species present in the sample. This approach allowed to precisely identify the ns changes of the spectra during the fluorescence decay of NAD(P)H in cardiomyocytes. Without any a priori knowledge of excited-state kinetics, the presence of each isoemissive point indicates the existence of two emitting species in the sample [62]. TRANES analysis of the cell AF in control conditions (Fig. 13.5b) revealed one isoemissive point at ~460 nm (see grey arrow at the Fig. 13.5b), pointing to two dominant spectral components with different decay kinetics, peaking around 430 nm (component 1) and 470 nm (component 2). In both cases, the component at longer wavelength rapidly faded in the first couple of ns, suggesting the presence of the process with the corresponding lifetime at the order of 1 ns or less; while the peak with shorter emission maximum was readily observable even after 5 ns of the decay. Most important components in the data were then identified by principal component analysis (PCA), while the component's most probable positions (spectral maxima) and thus their spectral profiles were determined by a target transformation technique (see [20] for details) following analysis of cell responses to metabolic modulators. With this approach, in addition to 2 components already present in control conditions (Fig. 13.4c): the 1st component peaking at 430–

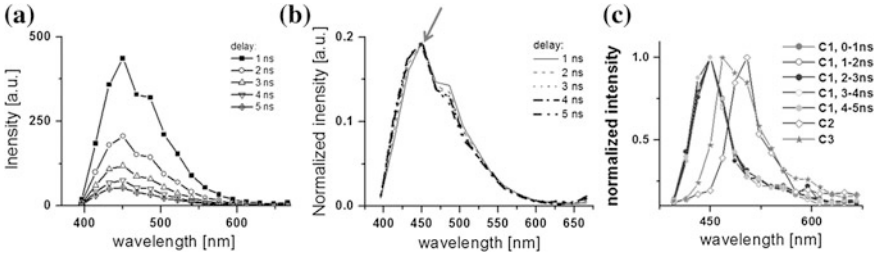

Fig. 13.5 Time-resolved, area-normalized emission spectroscopy (TRANES) of NAD(P)H fluorescence in a cardiac myocyte. (**a**, **b**) TRES and TRANES of cardiac cell AF in control conditions; *arrow* points to the isoemissive point. **c** Principal components resolved by PCA in living cardiac cells. Published in [33]

450 nm and the 2nd one with 450–470 nm spectral maximum, we also resolved 3rd significant spectral component with 510–530 nm spectral maximum (Fig. 13.5c), noted in some metabolic conditions only.

13.2.3 Separation of Individual NAD(P)H Fluorescence Components by Spectral Unmixing

To separate individual components in time-resolved NAD(P)H fluorescence, an original approach of time-resolved spectral decomposition was applied. Based on spectral decomposition of flavin fluorescence from spectrally-resolved TCSPC data [27], performed using spectral unmixing algorithms for multispectral imaging [37, 97], individual spectral components of NAD(P)H fluorescence recorded by multi-wavelength fluorescence lifetime spectroscopy were resolved in isolated cardiomyocytes [21, 31]. As featured at Fig. 13.6a, presence of three different components was confirmed with largest contribution of C1 and C2 to the overall fluorescence amplitude, as illustrated by spectrally unmixed fluorescence intensity for each component (Fig. 13.6b). A 0.5 ns steps served for the reconstitution of the fluorescence decay of each component using the sequential PCA over different time delays. Mono- or multi-exponential fit (Fig. 13.6c) was then applied to gather information on the fluorescence lifetime and amplitude of each resolved component: 1st (Fig. 13.6-C1), 2nd (Fig. 13.6-C2), and 3rd (Fig. 13.3-C3), respectively [31, 33]. Both components derived from NAD(P)H in organic and inorganic solvents presented mono-exponential decay. The 3rd component, corresponding to flavin fluorescence, was best fitted with double exponential decay; with its maximum at 520 nm, this component had little contribution to the overall photon counts at 450 nm. In addition to the Phasor (lifetime, spectral, or combined) approach [38, 42, 43, 83], this method thus represents a new tool to separate individual components in time-resolved fluorescence spectroscopy data, based on distinct spectral and lifetime characteristics, which are corresponding to precise molecules species.

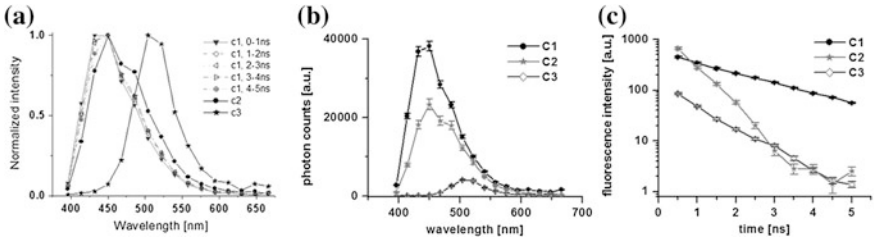

Fig. 13.6 Spectral decomposition of NAD(P)H fluorescence components in living cardiac cells. **a** Reference spectra selected as a base for spectral decomposition. **b** Photon counts calculated for each resolved component by area integration. **c** Fluorescence kinetics of the three spectral components (*C1*-1st component, *C2*-2nd component, *C3*-3rd component), estimated by spectral unmixing. The number of analyzed cells: n = 120; data are presented as mean ± SEM. Published in [21, 33]

13.2.4 Responses to Metabolic Modulation

In order to identify the nature of the resolved spectra, metabolic approach—similar to the chemiometric one—was employed. The sensitivity of the resolved components to changes in respiratory chain, in NADH production, as well as in lipid composition was tested in their cellular environment by evaluating the cell responsiveness to known metabolic regulators (Fig. 13.7 and Table 13.1) [33]. First, the sensitivity of the components to modulation of the mitochondrial respiratory chain was verified. On one hand, enhancement in the mitochondrial NADH content following restriction of the respiratory chain by Rotenone (1 μM), the Complex I inhibitor, significantly increased the fluorescence amplitude of both components (Fig. 13.7Ba, Bb), without notable effect on the fluorescence lifetimes (Fig. 13.7Aa, Ab). The addition of Na-cyanide (4 mM), the inhibitor of Complex IV, alone, or in the presence of Rotenone maintained higher fluorescence amplitudes of the two components. On the other hand, uncoupling ATP synthesis by DNP (50 μmol/L) or FCCP (200 nmol/L) lowered NAD(P)H content in cells, in accordance with a higher NADH dehydrogenation rate. This action was accompanied by change in the

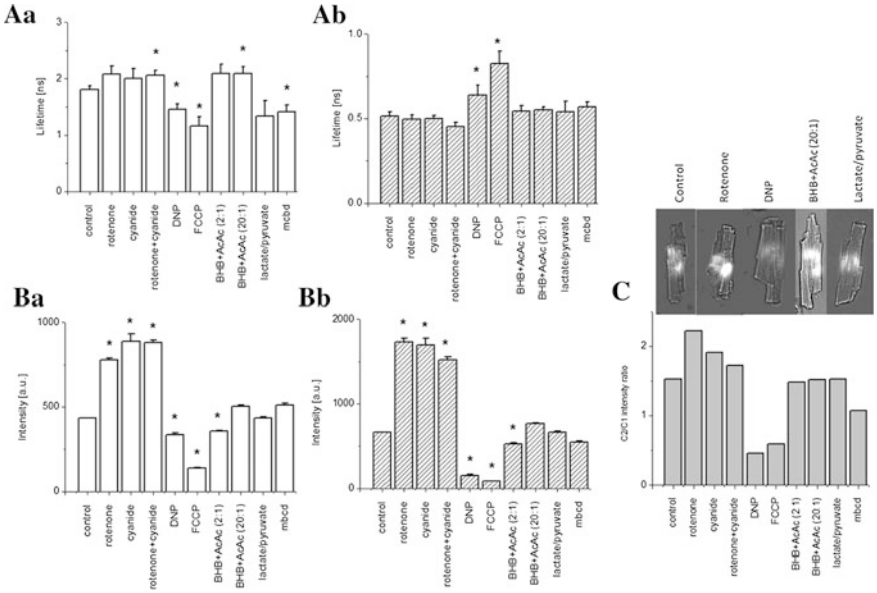

Fig. 13.7 Metabolic modulation of unmixed components. Estimated fluorescence lifetimes (**A**), together with calculated photon counts (**B**) of the resolved fluorescence component 1 (**a**) and component 2 (**b**) at 450 nm during metabolic modulation. (**C**) Ratio of the component 2 and component 1 amplitude with representative transmission image of the cell illumination in each condition. Data are shown as mean ± SEM, Control conditions (n = 120), Rotenone (1 μM; n = 30), Na-cyanide (4 mM; n = 10), NaCN+Rotenone (n = 15), DNP (50 μM; n = 15), fccp (200 nM; n = 20), after application of 20:1 (n = 35) or 2:1 BHB/AcAc (n = 18), lactate (2 mM) and pyruvate (100 μM; n = 10), MCβD (1 %; n = 10), *p < 0.05 versus control. Published in [33]

value of the fluorescence lifetime: decrease in the 1st, but increase in the 2nd resolved NAD(P)H component. These effects of modulators had repercussions also on the "free/bound" component amplitude ratio (Fig. 13.7c), which was proposed to correspond to NADH/NAD^+ reduction/oxidation pair [9, 75] and is thus an important indicator of mitochondrial metabolic status modifications.

Second, to promote mitochondrial NADH production as opposed to the one in the cytosol, BHB (3 mmol/L) was administered to cardiomyocytes in basic extracellular solution in the presence of different AcAc concentrations (Fig. 13.7): 1.5 mmol/L (ratio 2:1), closer to physiological conditions [76], and 150 μmol/L (ratio 20:1), to favour NADH production. As expected, increasing the BHB/AcAc ratio from 2:1 to 20:1, a condition favourable to NADH production, evoked rise in the amplitude of both 1st and 2nd component, in accordance with a higher NADH concentration in cardiomyocyte mitochondria, without affecting fluorescence lifetimes, or the component amplitudes ratio and thus mitochondrial redox potential. Third, to promote rise in the cytosolic NADH production, lactate (2 mmol/L) was administered in the presence of pyruvate (100 μmol/L) in concentrations found in the blood of studied animals [4]. This action had no significant effect on the fluorescence, indicating that the analyzed fluorescence signal is principally derived from the AF of mitochondria. Finally, the sensitivity of the resolved components to the presence of cholesterol in the cell membranes was also verified (Fig. 13.7). We noted that depletion of the cholesterol content with MCßD (1 %) [68] increased the fluorescence lifetime of the 1st component. These experiments demonstrated that the resolved components are selectively sensitive to changes in metabolic state, while pointing to higher specificity of the 1st lifetime component to lipid environment.

13.2.5 Perspectives in the Component Analysis: Data Classification

Presented analytical approach, based on spectral linear unmixing of individual component demonstrates how to resolve and determine precise molecular species present in a complex sample. However, the use of such procedure may not be always advantageous when data classification rather than evaluation of underlying molecular origins is required, as is often the case when rapid decision-making is needed, for example in clinical diagnostics. In this case, other methods for data classification can be considered. Estimation of spectral and/or time-resolved patterns associated with healthy versus diseases states is another mean to achieve classification of specific states and allow diagnostics of metabolic states in living cells and tissues. To classify metabolic state of living cells, classical approach based on spectral analysis can be employed, where the individual spectral components contributing to cell AF are estimated by blind source separation using non-negative matrix factorization [73]. This approach was demonstrated, for example, for flavin

fluorescence images of isolated cardiac cells in respect to responses to metabolic modulators [26]. However, in order to use an analytical approach better suited for fast data evaluation needed in situations such as clinical diagnostics, the classic classification method can be replaced by an advanced data analysis: the machine learning approach [70]. This approach is based on support vector machine with the set of the automatically calculated features from recorded spectral profile of spectral AF images. Our first results showed that machine learning can effectively classify the spectrally resolved flavin fluorescence images without the need of detailed knowledge about the sources of AF and their spectral properties [71]. This approach can also prove to be suitable for analysis of clinical data recorded by time-resolved fluorescence spectroscopy in the future.

13.3 Time-Resolved NAD(P)H Spectrometry in CVS Physiology

To introduce AF-assisted examination in cardiac myocytes for the CVS physiology studies, verification of NAD(P)H recordings in close-to-physiological conditions needs to be performed. In the case of living cardiac myocytes, this includes the modulation of AF during cells contraction and verification of the extent of photobleaching. In addition, to evaluate the methodology for investigation of metabolic changes during physiological LV remodelling, two conditions were chosen: NAD(P)H changes were investigated in the natural condition of pregnancy, while the effect of pharmaceutical drug was tested on a model drug—the Na pump inhibitor—ouabain.

13.3.1 Recordings in Contracting Myocytes

To evaluate changes of the metabolic oxidative state under physiological conditions, recording of NAD(P)H fluorescence was tested during cardiac cell contraction. Such recording is a complex technology problem. To solve this issue, we have designed a set-up [22] that allowed us to record rapid changes in AF during cell contraction stimulated by external platinum electrodes, incorporated in a home-made bath and triggered by a pulse generator at a frequency of 0.5 Hz (to stabilize sarcoplasmic reticulum loading), or 5 Hz (the rat heart rate) [4]. The basic timing sequence of the experiment is shown in Fig. 13.8, left.

The myocyte is stimulated periodically by an electrical pulse. After every stimulation pulse it contacts for a short period of time and then relaxes. Synchronously with the stimulation the ps diode laser is turned on for 100 ms via its ‘laser on’ signal. During the turn-un time the laser excites fluorescence and sends synchronisation pulses to the SPC-830 TCSPC module. The SPC-830 records only

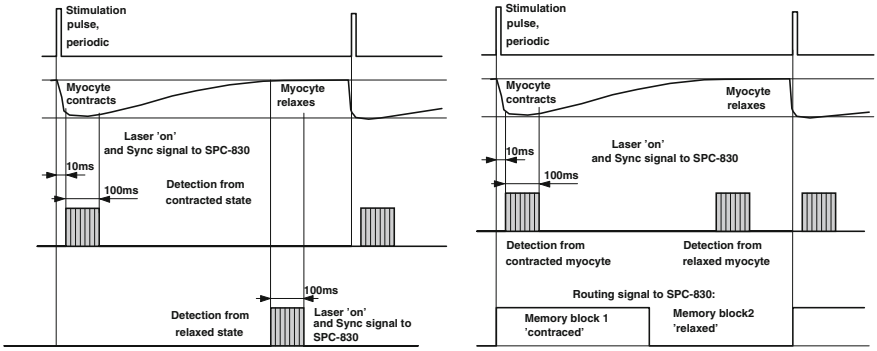

Fig. 13.8 Autofluorescence recording during cardiomyocyte contraction. *Left* Experiment timing, selection of myocyte state via temporal position of the Laser 'on' pulse in the stimulation period. *Right* Recording of contracted and relaxed state in the same stimulation period. Data are recorded into different memory blocks of TCSPC module by routing signal

when the synchronisation pulses are present. Fluorescence from different contraction states of the myocyte can thus be recorded by shifting the 'laser-on' pulse within the stimulation period.

Alternatively, the principle can be modified to record fluorescence from the contracted and the relaxed state in the same stimulation period, see Fig. 13.8, right. In that case, the laser is turned on both at the beginning (in the contracted state) and at the end (in the relaxed state) of the stimulation period. The data from the two states are routed into different memory blocks of the SPC-830 module by a (TTL) routing signal. Please see Chap. 1, Sects. 1.4.1 and 1.4.2 for routing principle.

We selected the relatively tiny illumination (laser-on) time due to the short length of the contraction cycle of a field-stimulated cardiac cell [32]. However, recording of fluorescence during such rapid process is problematic, as the fluorescence signal in 1 contraction cycle is insufficient to gather analysable data. We therefore accumulated the data over a large number of stimulation periods. Typically, we used a total collection time of 100 s (corresponding to the effective photon counting time of 100 s × 0.5 s^{-1} × 100 ms = 5 s). This approach allowed us to record a sufficient amount of emitted fluorescence in the 100-ms range, which is required to be able to study physiological behaviour of cardiomyocytes during their contraction.

Employing this setup, experiments can be performed at variable temperature (from room 24 °C to physiological 35 °C). The applicability of the newly developed setup was demonstrated by recording calcium transients at maximum contraction in cells loaded with the Fluo-3 fluorescent probe (excited by 475 nm pulsed picosecond diode laser) [22]. When time-resolved spectroscopy signals of flavin [22] or NAD(P)H [34] were evaluated during cell contraction at frequency 0.5 Hz, no significant change in the fluorescence at the peak of contraction and at rest was found. These results are in accordance with previously published observation that, during cell contraction, NADH levels have been shown not to change in single rat

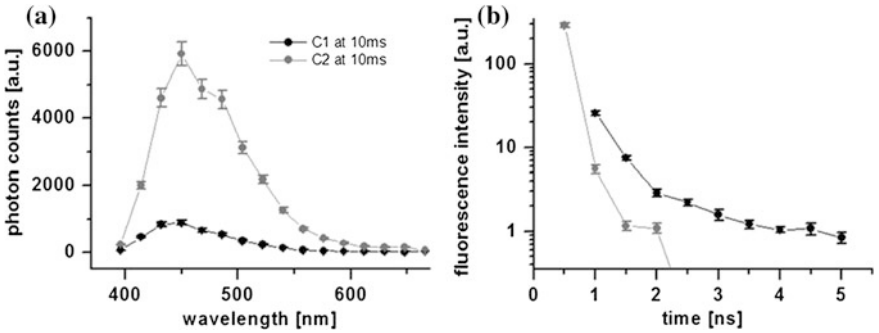

Fig. 13.9 Autofluorescence recording during cardiomyocyte contraction. *Left* NAD(P)H fluorescence photon counts calculated for the resolved component 1 and component 2 by area integration. *Right* Fluorescence kinetics of the two spectral components estimated by spectral unmixing in contracting cardiac myocytes (375 nm excitation, 0.5 Hz stimulation rate, room temperature, recorded at the peak of contraction, 10–110 ms, n = 15 cells). Data are shown as mean ± SEM. For more details, see [22, 34]

myocytes [49, 50, 90], while in trabeculae, a decrease in the fluorescence was seen [13]. Interestingly, as opposed to steady-state measurements, we noted more important contribution of the component 2 ("free NAD(P)H") when compared to the component 1 during contraction at 10 ms, see Fig. 13.9.

These experiments demonstrate the applicability of the time-resolved spectroscopy AF measurements under physiological conditions. They also confirmed that the use of repetitive scanning, synchronized to cell contraction, is a safe approach to gather dynamic information from these cells.

13.3.2 Photobleaching

Photobleaching, recorded following repetitive scanning, is a phenomenon that can significantly hamper fluorescence recordings and has to be monitored. It is considered to be closely related to two phenomena: photodamage and phototoxicity [63]. The level of photobleaching of NAD(P)H fluorescence was verified under our standard recording conditions (as described in Sect. 13.1.1). In these experiments, as illustrated in Fig. 13.10, NAD(P)H fluorescence was measured every minute for 30 s for the duration of 7 min, while the laser power was not modified. In order to precisely identify the effect of photobleaching, individual components of the NAD(P)H fluorescence were resolved by linear unmixing of the time-resolved spectroscopy signals, as described in Sect. 13.2 [33]. We identified comparable level of photobleaching of the two components [34] with the maintenance of the component amplitude ratio, which is a prerequisite for the correct estimation of metabolic state modifications. Low photobleaching rate is also a requirement for investigation of NAD(P)H changes during repetitive fluorescence recording performed in

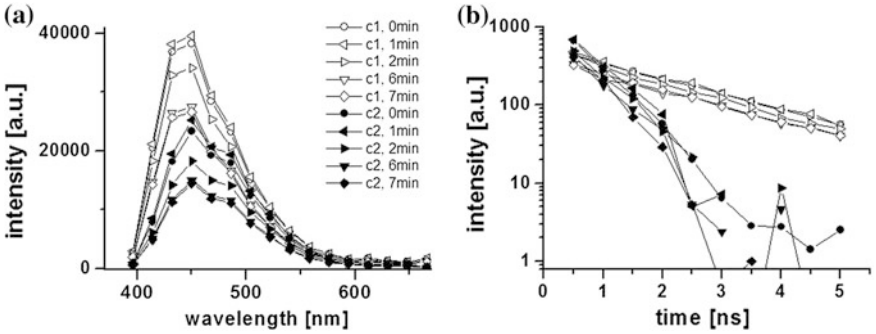

Fig. 13.10 Photobleaching of the two individual NAD(P)H fluorescence components. **a** Photon counts calculated by area integration and **b** fluorescence decays for each resolved component. Photobleaching was induced by excitation of a defocused elliptical spot with a 375 nm picosecond laser (~1 mW output power) for 30 s repeated every 60 s for 7 min. Detailed in [34]

experiments where cells were electrically stimulated to induce contractions (discussed in the Sect. 13.3.1). These results demonstrate that the application of time-resolved spectroscopy recording has much lesser effect on photobleaching than the confocal microscopy, for example, in agreement with previous observations that FLIM by TCSPC is less prone to bleaching than wide-field time-gating of frequency-domain FLIM [63], for example. These results confirmed that time-resolved spectroscopy recording by TCSPC is a safe method for monitoring metabolic oxidative state by means of recordings of endogenous fluorescence from live cells.

13.3.3 Cardiac Remodeling in Pregnancy

To investigate metabolic modifications under physiological conditions, a highly interesting physiological condition of pregnancy has been chosen as a model system. Normal pregnancy (P) induces significant CVS changes, associated with haemodynamic and endocrine modifications that contribute to maternal volume expansion and are necessary for fetal homeostasis and well being [60]. The heart remodeling observed during P resembles that seen in women during long-distance exercise training [48, 51], but there are important differences. Unlike endurance training [12], plasma hormones during P are modified and could affect cardiac function. Importantly, marked metabolic changes occur in this condition. Indeed, since the fetus has an absolute need for glucose, late P is associated with significant changes in carbohydrate metabolism [45], providing continuous nutrient availability to the developing fetus. This results in low blood glucose concentration, as well as in augmented levels of triglycerides and lactate in maternal blood [55, 56, 66]. In addition, in late P, basal oxidative metabolism is increased, leading to enhanced ATP demand with an elevated rate of mitochondrial NADH and oxidation [91]. P is characterized by metabolic remodeling of the mother's heart and by adaptations of haemodynamic and

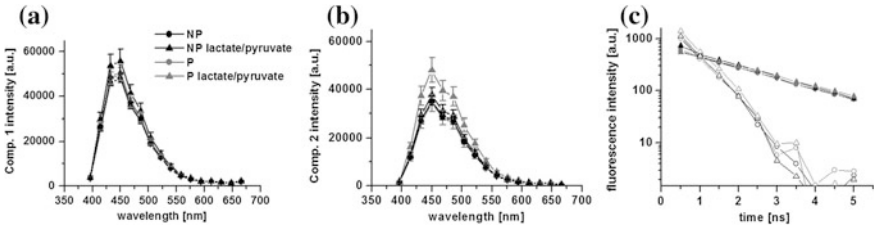

Fig. 13.11 NAD(P)H fluorescence in pregnancy. Photon counts calculated by area integration for the **a** component 1 and **b** component 2 resolved by linear unmixing of time-resolved spectroscopy data. Data are shown as mean ± SEM. **c** fluorescence decays for each resolved component. Presence of glucose (10 mmol/L) only (*circles*, n = 78 for NP, n = 26 for P), or in combination with lactate (2.0 mmol/L) and pyruvate (100 μmol/L) (*triangles*, n = 15 for NP, n = 15 for P) in NP (*black symbols*) versus P (*grey symbols*). For more details, see [3]

cardiac parameters. We demonstrated an adaptive hypertrophic cardiac remodeling during pregnancy, which includes cardiomyocyte dimensions and functions [3, 4]. Despite significant modifications in metabolism, we observed no modifications in the NAD(P)H fluorescence in control conditions in P (Fig. 13.11). Interestingly, spectrally-resolved lifetime detection of NAD(P)H fluorescence revealed modifications in metabolic oxidative state in the presence of substrates lactate/pyruvate that are naturally increased in P [4], mainly affecting the 2nd "free" NAD(P)H component (Fig. 13.11b). This result is in agreement with metabolic switch from glucose to lactate/pyruvte taking place in P.

13.3.4 Monitoring the Effect of the Pharmaceutical Drug Ouabain

AF has a great potential to monitor cellular responses to treatment by pharmaceutical drugs: non-invasive AF evaluation was employed by Hanley et al. [52] to measure reaction of NADH to volatile anesthetics halothane, isoflurane and sevoflurane. Rodrigo et al. [78] studied protective effects of 9,10-dinitrophenol on the cellular damage induced by metabolic inhibition and reperfusion in freshly isolated rat ventricular myocytes. We have tested the applicability of the method to evaluate the effect of pharmaceutical drug ouabain—the Na pump inhibitor—on the mitochondrial metabolic state [31, 39]. Ouabain was reported to decrease the NAD(P)H fluorescence in rat cardiac cells [67], but little information was available on mechanisms underlying this action. We demonstrated (Fig. 13.12) that the decrease in the time- and spectrally-resolved NAD(P)H fluorescence by ouabain was due to decrease in the "free" NAD(P)H fluorescence component leading to lowering of the free/bound NAD(P)H ratio, accompanied by reduced % of oxidized nucleotides, but increased NADH production in living cardiac myocytes [31]. Gathered findings suggest that ouabain induces a decrease in the cell oxidation. This information is

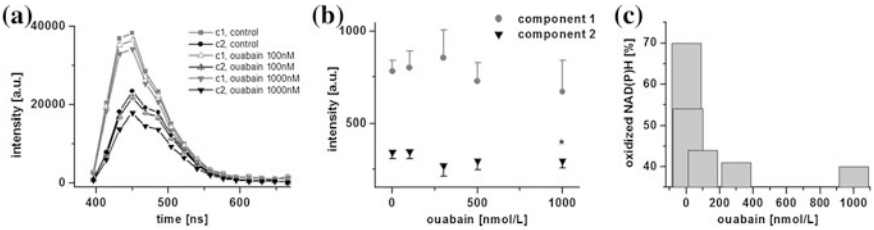

Fig. 13.12 Effect of pharmaceutical drug ouabain on metabolic state. **a** Photon counts calculated for each resolved NAD(P)H fluorescence component by area integration with rising ouabain concentrations. **b** Comparison of the effect of rising concentrations of ouabain on the integral NAD(P)H fluorescence intensity calculated for the component 1 (*black triangle*) and 2 (*grey circles*) at 450 nm spectral channel as the component amplitude multiplied by the unitary reference spectrum (data are shown as mean ± SEM, control (0 nM), n = 120; ouabain 100 nM, n = 36; ouabain 300–1000 nM, n = 15 *p < 0.05 vs. 0nM). **c** Concentration-dependent effect of ouabain on percentage of oxidized nucleotides is evaluated as [F(fully reduced) − Fcontrol]/[F(fully reduced) − F(fully oxidized)], where the fully reduced state is induced in the presence of Rotenone and the fully oxidized state is induced in the presence of DNP. Published in [31]

crucial for understanding of the effect of this pharmaceutical drug, particularly in regard to relationship between metabolic state and cardiac cell contractility [3].

The effect of ouabain was also studied in P, as circulating levels of cardiotonic steroids—endogenous Na pump inhibitors (which include ouabain)—are known to correlate with cardiac hypertrophy and/or changes in blood pressure [80], and are significantly elevated in pregnancy-induced hypertension (PIH) in women [69] as well as in experimental PIH (ePIH) in rats [41]. In normal P, inhibition of Na^+/K^+-ATPase has been suggested, namely via ouabain, to help plasma volume expansion [69]. In addition, Na^+/K^+-ATPase is known to be regulated by angiotensin and aldosterone, increased in normal P, but blunted in PIH and ePIH [72]. In cardiac myocytes, Na pump inhibition regulates not only excitation-contraction coupling via $[Na^+]_i$-stimulated reverse sodium/calcium exchange [93], but also cardiomyocyte metabolism, including the Ras-Rac-NAD(P)H oxidase cascade [94]. We demonstrated that P affected the action of ouabain on NAD(P)H fluorescence [39]. Altogether, these results demonstrated that the time-resolved spectroscopy of NAD(P)H can be highly valuable also for testing the effect of pharmaceutical drugs on cellular metabolism in physiological conditions.

13.4 Time-Resolved NAD(P)H Spectrometry in CVS Pathology

Numerous diseases of the heart, including hypertension and diabetes, are often linked to alterations in mitochondrial energy metabolism associated with the mitochondrial dysfunction [36]. Chronic alterations of fuel metabolism and oxidative stress status are factors that could impair the capacity of mitochondria to fulfil their

crucial role in energy production [65] and thereby contribute to the activation of pathways governing cell death and/or disease [11, 35]. This creates room for numerous applications of non-invasive AF measurements in identification and study of CVS pathology. Effects of oxidative stress were tested together with the study of cardiomyocyte AF under conditions of pathological pregnancy. Clinical applications of time-resolved spectroscopy of NAD(P)H in cardiac myocyte was demonstrated in the case of diagnostics of early stages of cardiac allograft rejection.

13.4.1 Evaluation of the Effect of Oxidative Stress

Oxidative stress is a condition resulting from imbalance between oxidized and reduced species [79]. Lipid peroxidation is a major biochemical consequence of the oxidative deterioration of polyunsaturated lipids in cell membranes and causes damage to membrane integrity and loss of protein function. One of the most reactive products of n-6 polyunsaturated fatty acid peroxidation of membrane phospholipids is 4-hydroxy-2-nonenal (HNE), the primary α,β-unsaturated hydroxyalkenal formed in cells by LPO process [40]. HNE is generated in the peroxidation of lipids containing polyunsaturated omega-6 acyl groups, such as arachidonic or linoleic acids, and of the corresponding fatty acids. In cardiac myocytes, HNE has been shown capable of affecting NADPH production by inactivating mitochondrial $NADP^+$-isocitrate dehydrogenase activity, an important enzyme that controls redox and energy status [7, 8, 96]. The sensitivity of NAD(P)H fluorescence to oxidative stress was tested and proved using stressors such as hydrogen peroxide (H_2O_2) or HNE in living LV myocytes (see Supplement in [3] for details). The effect of HNE was evaluated on the NAD(P)H content in order to better understand mechanisms underlying the lipid peroxidation action. In these experiments, cells were pre-heated to 35 °C to mimic effects at physiological temperatures. Gathered results demonstrated that HNE reduces cell NAD(P)H content (Fig. 13.13) via decrease in the production of NADH and stimulation of the NAD(P)H use by flavoprotein complexes [29]. Consequently, HNE provoked an important cell oxidation by dehydrogenation of both free and bound NAD(P)H molecules in living cardiac cells. This action is likely to affect the overall energy production and use in the heart. These findings not only shed a new light on the effect of HNE on the regulation of NAD(P)H in living cardiac cells, but also demonstrated that oxidative stress via NADPH pathway can have significant effect on the AF measurement and, consequently, has to be taken into account in the analysis of AF signals.

13.4.2 Pathological Pregnancy

Heart disease remains an important cause of women's mortality [84]. Pregnancy induced hypertension was proved to be a predictor of CV disease for women later in

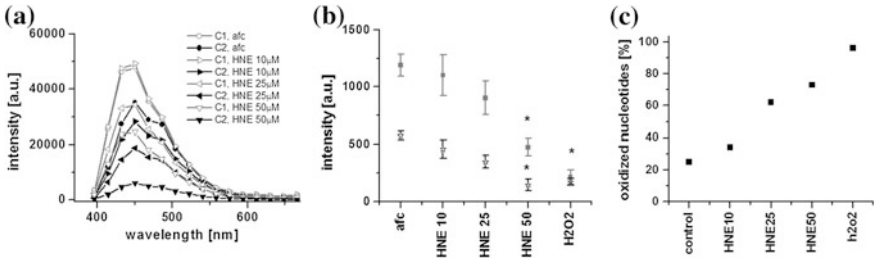

Fig. 13.13 Effect of HNE on NAD(P)H fluorescence. **a** Photon counts calculated for each resolved component by area integration in the presence of rising HNE concentrations. **b** Concentration-dependent effect of HNE on the integral NAD(P)H fluorescence intensity of the component 1 (*black asterisks*) and 2 (*grey squares*), calculated at the 450 nm spectral channel as the component amplitude multiplied by the unitary reference spectrum; data are shown as mean ± SEM, control, n = 78 cells; HNE, 25 µM, n = 71; HNE, 50 µM, n = 19; *$p < 0.05$ versus control. **c** Percentage of oxidized nucleotides, calculated as fluorescence at (fully reduced − control)/(fully reduced − fully oxidized) state in different HNE concentrations and/or in the presence of H_2O_2. Published in [29]

their lives [81, 92]. In so far as cardiac changes are concerned, maternal heart rate is one of the earliest to increase in P, followed by augmented blood volume. Hypervolemia is the result of active sodium and water retention because of alterations in osmoregulation and the renin-angiotensin-aldosterone system [45], accompanied by decreased sodium serum levels of about 3–4 mM in humans [53] as well as in rats [6]. Subsequently, cardiac output rises together with stroke volume in response to elevated heart rate and reaches maximum values in the final stages of delivery, placing increased volume load on the heart. Blood volume expansion leads to myocardial adaptations mainly affecting the LV, which is more susceptible to heightened load. In contrast to pathological conditions, these alterations are associated with physiological reduction of blood pressure and are reversible. Our work demonstrated that while adaptive compensated cardiomyocyte remodeling is present in normal P in rats, maladaptive components were identified in the model of experimental pregnancy-induced-hypertension [4].

In this setting, mineralocorticoid hormones, including aldosterone of the renin-angiotensin-aldosterone chain, play an important but poorly understood role. Aldosterone is markedly elevated during P [14, 15]; this steroid hormone controls blood volume, and its rise contributes to maternal volume expansion [60]. Mineralocorticoid receptors are expressed in the heart of humans and rodents [77], indicating possible involvement on cardiac metabolic adaptations. Glucocorticoid-mineralocorticoid complexes have been proposed to be activated by lowered NADH level, a determinant of the redox state, and/or by reactive oxygen species [44]. We have tested the effect of mineralocorticoid inhibitor canrenoate in P (P_{can}). These experiments demonstrated that responsiveness of cardiomyocytes to lactate/pyruvate (Fig. 13.2), was modified by canrenoate (Fig. 13.14), (see also Supplementary material in [3]) due to regulation of the "free" NAD(P)H, pointing to the possible role of this hormone in metabolic remodeling that takes place in

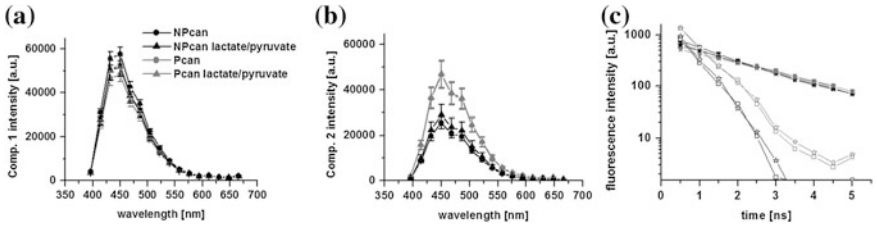

Fig. 13.14 Effect of lactate/pyruvate in MR-Inhibitor canrenoate treated rats. **a** NAD(P)H fluorescence component 1 and **b** component 2 resolved by linear unmixing of time-resolved spectroscopy data. Data are shown as mean ± SEM. **c** Fluorescence decays for each resolved component. Presence of glucose (10 mmol/L) only (*squares*, n = 20 for NP_{can}, n = 20 for P_{can}), or in combination with lactate (2.0 mmol/L) and pyruvate (100 μmol/L) (*asterisks*, n = 10 for NP_{can}, n = 25 for P_{can}) in NP_{can} (*black symbols*) versus NP_{can} (*grey symbols*). For more details, see [3]

P [3]. Gathered finding, together with the ones on the Na pump inhibitor ouabain opened a completely new chapter of investigation of P as a highly interesting metabolic condition, also recognized by the Judith Heiny's editorial in Experimental Physiology [54].

13.4.3 Monitoring Rejection of Transplanted Hearts

Transfer of gathered knowledge to clinics is a crucial part of the technology application. We have tested possibility of such knowledge transfer to evaluate early stages of cardiac rejection in paediatric patients with transplanted hearts. Cardiac allograft rejection involves several processes, including activation and proliferation of T-lymphocyte subsets (leading to lymphocyte infiltration and immune destruction of graft tissue), as well as graft vessel injury and thrombosis [57]. Although molecular mechanisms of the rejection remain unclear, alloantigen-dependent and -independent factors are known contributors [87]. Ischemia-reperfusion injury is the most influential alloantigen-independent factor [47], resulting in cardiac cell hypoxia. Such modifications, which also include alterations in the cell oxidative metabolism, often develop rapidly. Some observations suggest that cardiac cells undergo modifications in their oxidative state with the progression of cardiac rejection [85, 86], namely as a result of cell hypoxia, following ischemic changes of cardiac cells. Evaluation of the oxidative metabolism can thus serve as an early indication of the rejection of transplanted hearts.

Time-resolved NAD(P)H fluorescence spectroscopy was therefore attempted in examination of transplanted tissues. A strong correlation between changes in AF spectra and the rejection grade were found in rat heart allograft model [74], but more difficulties were encountered using human tissues [95], possibly due to use of frozen fractions. When time-resolved NAD(P)H spectroscopy method was applied to human cardiac cells freshly isolated from endomyocardial biopsy tissue

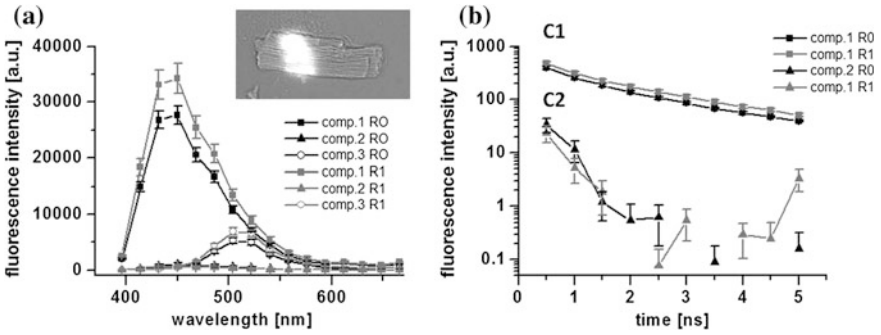

Fig. 13.15 Effect of rejection on NAD(P)H fluorescence in transplanted hearts. **a** NAD(P)H emission spectra determined as total photon counts in human cardiomyocytes isolated from cardiac biopsy of heart transplanted patients presenting no rejection (*R0*) or mild rejection (*R1*) (recording time 30 s, excitation at 375 nm; in the inset, illustrative picture of the recorded human cardiac myocyte: the *bright* spot corresponds to a fluorescence excited by a defocused laser beam used for recording). **b** NAD(P)H fluorescence decays of the component 1 (*C1*) and component 2 (*C2*), resolved after linear unmixing in human cardiomyocytes and compared in *R0* and *R1*. Data are shown as mean ± SEM; R0, n = 48 cells; R1, n = 35 cells. Published in [21]

(Fig. 13.15a), an increase in NAD(P)H fluorescence in the hearts of transplanted paediatric patients was detected (Fig. 13.15b) [19, 21]. Spectral unmixing revealed that from the two NAD(P)H components present in human cardiomyocytes [21], mild rejection of transplanted hearts in paediatric patients affected primarily the lifetimes of the first C1 component (Fig. 13.15-C1, C2). This result not only explained higher NAD(P)H fluorescence intensities, but also proved the applicability of the time-resolved AF spectroscopy as a non-invasive diagnostic tool directly in clinics. At the same time, it also showed difficulties to resolve individual components in the clinical data and prompted search for other advanced data classification approaches, as discussed in Sect. 13.2.

Acknowledgements Supported by Integrated Initiative of European Laser Infrastructures LaserLab Europe III (EC's FP7 under grant agreement no 284464) and the Research grant agency of the Slovak Research and Development Agency APVV-0242-11. Part of this work was presented as doctoral dissertation thesis of AC. I would like to thank Y. Cheng for the preparation of Table 13.1.

References

1. S. Aneba, Y. Cheng, A. Mateasik, B. Comte, D. Chorvat, A. Chorvatova, Probing of cardiomyocyte metabolism by spectrally resolved lifetime detection of NAD(P)H fluorescence. Comput. in Cardiol. **34**, 349–352 (2007)
2. S.W. Ballinger, Mitochondrial dysfunction in cardiovascular disease. Free Radic. Biol. Med. **38**, 1278–1295 (2005)

3. V. Bassien-Capsa, F.M. Elzwiei, S. Aneba, J.C. Fouron, B. Comte, A. Chorvatova, Metabolic remodelling of cardiac myocytes during pregnancy: the role of mineralocorticoids. Can. J. Cardiol. **27**, 834–842 (2011)
4. V. Bassien-Capsa, J.C. Fouron, B. Comte, A. Chorvatova, Structural, functional and metabolic remodeling of rat left ventricular myocytes in normal and in sodium-supplemented pregnancy. Cardiovasc. Res. **69**, 423–431 (2006)
5. M.C. Battista, E. Calvo, A. Chorvatova, B. Comte, J. Corbeil, M. Brochu, Intra-uterine growth restriction and the programming of left ventricular remodelling in female rats. J. Phys. Lond. **565**, 197–205 (2005)
6. A. Beausejour, K. Auger, J. St. Louis, M. Brochu, High-sodium intake prevents pregnancy-induced decrease of blood pressure in the rat. Am. J. Physiol. Heart Circ. Physiol. **285**, H375–H383 (2003)
7. M. Benderdour, G. Charron, B. Comte, R. Ayoub, D. Beaudry, S. Foisy, D. Deblois, C. Des Rosiers, Decreased cardiac mitochondrial NADP+-isocitrate dehydrogenase activity and expression: a marker of oxidative stress in hypertrophy development. Am. J. Physiol. Heart Circ. Physiol. **287**, H2122–H2131 (2004)
8. M. Benderdour, G. Charron, D. Deblois, B. Comte, C. Des Rosiers, Cardiac mitochondrial NADP+-isocitrate dehydrogenase is inactivated through 4-hydroxynonenal adduct formation: an event that precedes hypertrophy development. J. Biol. Chem. **278**, 45154–45159 (2003)
9. D.K. Bird, L. Yan, K.M. Vrotsos, K.W. Eliceiri, E.M. Vaughan, P.J. Keely, J.G. White, N. Ramanujam, Metabolic mapping of MCF10A human breast cells via multiphoton fluorescence lifetime imaging of the coenzyme NADH. Cancer Res. **65**, 8766–8773 (2005)
10. K. Blinova, S. Carroll, S. Bose, A.V. Smirnov, J.J. Harvey, J.R. Knutson, R.S. Balaban, Distribution of mitochondrial NADH fluorescence lifetimes: steady-state kinetics of matrix NADH interactions. Biochemistry **44**, 2585–2594 (2005)
11. V. Borutaite, G.C. Brown, Mitochondria in apoptosis of ischemic heart. FEBS Lett. **541**, 1–5 (2003)
12. R.W. Braith, M.A. Welsch, M.S. Feigenbaum, H.A. Kluess, C.J. Pepine, Neuroendocrine activation in heart failure is modified by endurance exercise training. J. Am. Coll. Cardiol. **34**, 1170–1175 (1999)
13. R. Brandes, D.M. Bers, Increased work in cardiac trabeculae causes decreased mitochondrial NADH fluorescence followed by slow recovery. Biophys. J. **71**, 1024–1035 (1996)
14. M. Brochu, J.P. Gauvin, J. St. Louis, Increase of aldosterone secretion in adrenal cortex suspensions derived from pregnant rats. Proc. Soc. Exp. Biol. Med. **212**, 147–152 (1996)
15. M. Brochu, J.G. Lehoux, S. Picard, Effects of gestation on enzymes controlling aldosterone synthesis in the rat adrenal. Endocrinology **138**, 2354–2358 (1997)
16. B. Chance, B. Schoener, R. Oshino, F. Itshak, Y. Nakase, Oxidation-reduction ratio studies of mitochondria in freeze-trapped samples. NADH and flavoprotein fluorescence signals. J. Biol. Chem. **254**, 4764–4771 (1979)
17. B. Chance, B. Thorell, Fluorescence measurements of mitochondrial pyridine nucleotide in aerobiosis and anaerobiosis. Nature **184**, 931–934 (1959)
18. Y. Cheng, N. Dahdah, N. Porier, J. Miro, D. Chorvat Jr., A. Chorvatova, Spectrally and time-resolved study of NADH autofluorescence in cardiac myocytes from human biopsies. Proc. SPIE: Int. Soc. Opt. Eng. **6771**, 677104-1–677104-13 (2007)
19. Y. Cheng, A. Mateasik, N. Dahdah, N. Poirier, J. Miro, D. Jr. Chorvat, A. Chorvatova, Analysis of NAD(P)H fluorescence components in cardiac myocytes from human biopsies: a new tool to improve diagnostics of rejection of transplanted patients. Proc. SPIE: Int. Soc. Opt. Eng. **7183**, 718319–1-718319-8 (2009)
20. D. Chorvat Jr., A. Chorvatova, Spectrally resolved time-correlated single photon counting: a novel approach for characterization of endogenous fluorescence in isolated cardiac myocytes. Eur. Biophys. J. Biophys. Lett. **36**, 73–83 (2006)
21. D. Chorvat Jr., A. Mateasik, Y. Cheng, N. Poirier, J. Miro, N.S. Dahdah, A. Chorvatova, Rejection of transplanted hearts in patients evaluated by the component analysis of multi-wavelength NAD(P)H fluorescence lifetime spectroscopy. J. Biophotonics **3**, 646–652 (2010)

22. D. Chorvat Jr., S. Abdulla, F. Elzwiei, A. Mateasik, A. Chorvatova, Screening of cardiomyocyte fluorescence during cell contraction by multi-dimensional TCSPC. Proc. SPIE: Int. Soc. Opt. Eng. **6860**, 686029-1–686029-12 (2008)
23. D. Chorvat Jr., V. Bassien-Capsa, M. Cagalinec, J. Kirchnerova, A. Mateasik, B. Comte, A. Chorvatova, Mitochondrial autofluorescence induced by visible light in single rat cardiac myocytes studied by spectrally resolved confocal microscopy. Laser Phys. **14**, 220–230 (2004)
24. D. Chorvat Jr., A. Chorvatova, Study of flavins in living cardiomyocytes using spectrally resolved time correlated single photon counting. J. Mol. Cell. Cardiol. **39**, 187 (2005)
25. D. Chorvat Jr., A. Chorvatova, Multi-wavelength fluorescence lifetime spectroscopy: a new approach to the study of endogenous fluorescence in living cells and tissues. Laser Phys. Lett. **6**, 175–193 (2009)
26. D. Chorvat Jr., J. Kirchnerova, M. Cagalinec, J. Smolka, A. Mateasik, A. Chorvatova, Spectral unmixing of flavin autofluorescence components in cardiac myocytes. Biophys. J. **89**, L55–L57 (2005)
27. D. Chorvat Jr., A. Mateasik, J. Kirchnerova, A. Chorvatova, Application of spectral unmixing in multi-wavelength time-resolved spectroscopy. Proc. SPIE: Int. Soc. Opt. Eng. **6771**, 677105-1–677105-12 (2007)
28. A.M. Chorvatova, in *Natural Biomarkers for Cellular Metabolism: Biology, Techniques and Applications,* ed. by A.A. Heikal, V. Ghukasyan. Autofluorescence-assisted examination of cardiovascular system physiology and pathology (Taylor and Francis, Boca Raton, 2014), pp. 245–271
29. A. Chorvatova, S. Aneba, A. Mateasik, D. Chorvat, B. Comte, Time-resolved fluorescence spectroscopy investigation of the effect of 4-hydroxynonenal on endogenous NAD(P)H in living cardiac myocytes. J. Biomed. Opt. **18**, 67009 (2013)
30. A. Chorvatova, D. Chorvat, Jr., Tissue fluorophores and their spectroscopic characteristics, in *Fluorescence Lifetime Spectroscopy and Imaging for Tissue Biomedical Diagnostics*, ed. by L. Marcu, P. French, D. Elson, (CRC Press, Boca Raton, 2014), pp. 47–84
31. A. Chorvatova, F. Elzwiei, A. Mateasik, D. Chorvat Jr., Effect of ouabain on metabolic oxidative state in living cardiomyocytes evaluated by time-resolved spectroscopy of endogenous NAD(P)H fluorescence. J. Biomed. Opt. **17**, 101505 (2012)
32. A. Chorvatova, G. Hart, M. Hussain, Na(+)/Ca(2+) exchange current (I(Na/Ca)) and sarcoplasmic reticulum Ca(2+) release in catecholamine-induced cardiac hypertrophy. Cardiovasc. Res. **61**, 278–287 (2004)
33. A. Chorvatova, A. Mateasik, D. Chorvat Jr., Spectral decomposition of NAD(P)H fluorescence components recorded by multi-wavelength fluorescence lifetime spectroscopy in living cardiac cells. Laser Phys. Lett. **10**, 125703 (2013)
34. A. Chorvatova, A. Mateasik, D. Chorvat Jr., Laser-induced photobleaching of NAD(P)H fluorescence components in cardiac cells resolved by linear unmixing of TCSPC signals, pp. 790326-1–790326-9 (2011)
35. S. Cortassa, M.A. Aon, E. Marban, R.L. Winslow, B. O'Rourke, An integrated model of cardiac mitochondrial energy metabolism and calcium dynamics. Biophys. J. **84**, 2734–2755 (2003)
36. N.S. Dhalla, N. Afzal, R.E. Beamish, B. Naimark, N. Takeda, M. Nagano, Pathophysiology of cardiac dysfunction in congestive heart failure. Can. J. Cardiol. **9**, 873–887 (1993)
37. M.E. Dickinson, G. Bearman, S. Tilie, R. Lansford, S.E. Fraser, Multi-spectral imaging and linear unmixing add a whole new dimension to laser scanning fluorescence microscopy. Biotechniques **31**, 1272–1276 (2001)
38. M.A. Digman, V.R. Caiolfa, M. Zamai, E. Gratton, The phasor approach to fluorescence lifetime imaging analysis. Biophys. J. **94**, L14–L16 (2008)
39. F. Elzwiei, V. Bassien-Capsa, J. St-Louis, A. Chorvatova, Regulation of the sodium pump during cardiomyocyte adaptation to pregnancy. Exp. Physiol. **98**, 183–192 (2013)
40. H. Esterbauer, R.J. Schaur, H. Zollner, Chemistry and biochemistry of 4-hydroxynonenal, malonaldehyde and related aldehydes. Free Radic. Biol. Med. **11**, 81–128 (1991)

41. O.V. Fedorova, N.I. Kolodkin, N.I. Agalakova, A.R. Namikas, A. Bzhelyansky, J. St. Louis, E.G. Lakatta, A.Y. Bagrov, Antibody to marinobufagenin lowers blood pressure in pregnant rats on a high NaCl intake, J. Hypertens. **23**, 835–842 (2005)
42. F. Fereidouni, A.N. Bader, H.C. Gerritsen, Spectral phasor analysis allows rapid and reliable unmixing of fluorescence microscopy spectral images. Opt. Express **20**, 12729–12741 (2012)
43. F. Fereidouni, K. Reitsma, H.C. Gerritsen, High speed multispectral fluorescence lifetime imaging. Opt. Express **21**, 11769–11782 (2013)
44. J.W. Funder, RALES, EPHESUS and redox. J. Steroid Biochem. Mol. Biol. **93**, 121–125 (2005)
45. S.G. Gabbe, J.R. Niebyl, J.L. Simpson, in *Obstetrics. Normal and Problem Pregnancies*, ed. by S. G. Gabbe, J.R. Niebyl, J.L. Simpson,(Churchill Livingstone, A Harcourt Health Science Company, U.S.A., Philadelphia, Pennsylvania, 2002)
46. A. Gafni, L. Brand, Fluorescence decay studies of reduced nicotinamide adenine dinucleotide in solution and bound to liver alcohol dehydrogenase. Biochemistry **15**, 3165–3171 (1976)
47. P.B. Gaudin, B.K. Rayburn, G.M. Hutchins, E.K. Kasper, K.L. Baughman, S.N. Goodman, L.E. Lecks, W.A. Baumgartner, R.H. Hruban, Peritransplant injury to the myocardium associated with the development of accelerated arteriosclerosis in heart transplant recipients. Am. J. Surg. Pathol. **18**, 338–346 (1994)
48. L.E. Ginzton, R. Conant, M. Brizendine, M.M. Laks, Effect of long-term high intensity aerobic training on left ventricular volume during maximal upright exercise. J. Am. Coll. Cardiol. **14**, 364–371 (1989)
49. E.J. Griffiths, H. Lin, M.S. Suleiman, NADH fluorescence in isolated guinea-pig and rat cardiomyocytes exposed to low or high stimulation rates and effect of metabolic inhibition with cyanide. Biochem. Pharmacol. **56**, 173–179 (1998)
50. E.J. Griffiths, S.K. Wei, M.C. Haigney, C.J. Ocampo, M.D. Stern, H.S. Silverman, Inhibition of mitochondrial calcium efflux by clonazepam in intact single rat cardiomyocytes and effects on NADH production. Cell Calcium **21**, 321–329 (1997)
51. M. Guazzi, F.C. Musante, H.L. Glassberg, J.R. Libonati, Detection of changes in diastolic function by pulmonary venous flow analysis in women athletes. Am. Heart J. **141**, 139–147 (2001)
52. P.J. Hanley, J. Ray, U. Brandt, J. Daut, Halothane, isoflurane and sevoflurane inhibit NADH: ubiquinone oxidoreductase (complex I) of cardiac mitochondria. J. Physiol. **544**, 687–693 (2002)
53. A.P. Heenan, L.A. Wolfe, G.A. Davies, M.J. McGrath, Effects of human pregnancy on fluid regulation responses to short-term exercise. J. Appl. Physiol. **95**, 2321–2327 (2003)
54. J. Heiny, Pumped up and pregnant. Exp. Physiol. **98**, 48 (2013)
55. E. Herrera, M.A. Lasuncion, M. Palacin, A. Zorzano, B. Bonet, Intermediary metabolism in pregnancy. First theme of the Freinkel era. Diabetes **40**(2), 83–88 (1991)
56. E. Herrera, H. Ortega, G. Alvino, N. Giovannini, E. Amusquivar, I. Cetin, Relationship between plasma fatty acid profile and antioxidant vitamins during normal pregnancy. Eur. J. Clin. Nutr. **58**, 1231–1238 (2004)
57. F.M. Hoffman, Outcomes and complications after heart transplantation: a review. J. Cardiovasc. Nurs. **20**, S31–S42 (2005)
58. J. Horilova, Z. Tomaskova, M. Grman, A. Ilesova, M. Bucko, A. Vikartovska, P. Gemeiner, V. Stefuca, I. Lajdova, D. Chorvat, A. Chorvatova, Monitoring metabolic oxidative state in living cells and systems using time-resolved fluorescence and spectroscopy techniques. Proc. ADEPT 131–134 (2013)
59. S. Huang, A.A. Heikal, W.W. Webb, Two-photon fluorescence spectroscopy and microscopy of NAD(P)H and flavoprotein. Biophys. J. **82**, 2811–2825 (2002)
60. E. Jensen, C. Wood, M. Keller-Wood, The normal increase in adrenal secretion during pregnancy contributes to maternal volume expansion and fetal homeostasis. J. Soc. Gynecol. Investig. **9**, 362–371 (2002)
61. J.R. Knutson, J.M. Beechem, L. Brand, Simultaneous analysis of multiple fluorescence decay curves: a global approach. Chem. Phys. Lett. **102**, 501–507 (1983)

62. A.S.R. Koti, M.M. Krishna, N. Periasamy, Time-resolved area-normalized emission spectroscopy (TRANES): a novel method for confirming emission from two excited states. J. Phys. Chem. A **105**, 1767–1771 (2001)
63. S. Kumar, C. Dunsby, P.A. De Beule, D.M. Owen, U. Anand, P.M. Lanigan, R.K. Benninger, D.M. Davis, M.A. Neil, P. Anand, C. Benham, A. Naylor, P.M. French, Multifocal multiphoton excitation and time correlated single photon counting detection for 3-D fluorescence lifetime imaging. Opt. Express **15**, 12548–12561 (2007)
64. J.R. Lakowicz, On spectral relaxation in proteins. Photochem. Photobiol. **72**, 421–437 (2000)
65. E.J. Lesnefsky, S. Moghaddas, B. Tandler, J. Kerner, C.L. Hoppel, Mitochondrial dysfunction in cardiac disease: ischemia–reperfusion, aging, and heart failure. J. Mol. Cell. Cardiol. **33**, 1065–1089 (2001)
66. A. Leturque, S. Hauguel, J.P. Revelli, A.F. Burnol, J. Kande, J. Girard, Fetal glucose utilization in response to maternal starvation and acute hyperketonemia. Am. J. Physiol. **256**, E699–E703 (1989)
67. T. Liu, D.A. Brown, B. O'Rourke, Role of mitochondrial dysfunction in cardiac glycoside toxicity. J. Mol. Cell. Cardiol. **49**, 728–736 (2010)
68. T. Loftsson, P. Jarho, M. Masson, T. Jarvinen, Cyclodextrins in drug delivery. Expert Opin. Drug Deliv. **2**, 335–351 (2005)
69. D.A. Lopatin, E.K. Ailamazian, R.I. Dmitrieva, V.M. Shpen, O.V. Fedorova, P.A. Doris, A.Y. Bagrov, Circulating bufodienolide and cardenolide sodium pump inhibitors in preeclampsia. J. Hypertens. **17**, 1179–1187 (1999)
70. J. Luts, F. Ojeda, R. Van de Plas, M.B. De, H.S. Van, J.A. Suykens, A tutorial on support vector machine-based methods for classification problems in chemometrics. Anal. Chim. Acta **665**, 129–145 (2010)
71. A. Mateasik, D. Chorvat, A. Chorvatova, Analysis of spectrally resolved autofluorescence images by support vector machines. Proc. SPIE **8588**, 85882J-1–85882J-10 (2013)
72. A.S. Mihailidou, H. Bundgaard, M. Mardini, P.S. Hansen, K. Kjeldsen, H.H. Rasmussen, Hyperaldosteronemia in rabbits inhibits the cardiac sarcolemmal Na(+)- K(+) pump. Circ. Res. **86**, 37–42 (2000)
73. A.S. Montcuquet, L. Herve, F. Navarro, J.M. Dinten, J.I. Mars, Nonnegative matrix factorization: a blind spectra separation method for in vivo fluorescent optical imaging. J. Biomed. Opt. **15**, 056009 (2010)
74. D.C. Morgan, J.E. Wilson, C.E. MacAulay, N.B. MacKinnon, J.A. Kenyon, P.S. Gerla, C. Dong, H. Zeng, P.D. Whitehead, C.R. Thompson, B.M. McManus, New method for detection of heart allograft rejection: validation of sensitivity and reliability in a rat heterotopic allograft model. Circulation **100**, 1236–1241 (1999)
75. R. Niesner, B. Peker, P. Schlusche, K.H. Gericke, Noniterative biexponential fluorescence lifetime imaging in the investigation of cellular metabolism by means of NAD(P)H autofluorescence. ChemPhysChem **5**, 1141–1149 (2004)
76. L.H. Opie, P. Owen, Effects of increased mechanical work by isolated perfused rat heart during production or uptake of ketone bodies. Assessment of mitochondrial oxidized to reduced free nicotinamide-adenine dinucleotide ratios and oxaloacetate concentrations. Biochem. J. **148**, 403–415 (1975)
77. P. Pearce, J.W. Funder, High affinity aldosterone binding sites (type I receptors) in rat heart. Clin. Exp. Pharmacol. Physiol **14**, 859–866 (1987)
78. G.C. Rodrigo, C.L. Lawrence, N.B. Standen, Dinitrophenol pretreatment of rat ventricular myocytes protects against damage by metabolic inhibition and reperfusion. J. Mol. Cell. Cardiol. **34**, 555–569 (2002)
79. C.X. Santos, N. Anilkumar, M. Zhang, A.C. Brewer, A.M. Shah, Redox signaling in cardiac myocytes. Free Radic. Biol. Med. **50**, 777–793 (2011)
80. W. Schoner, Endogenous digitalis-like factors. Clin. Exp. Hypertens. A **14**, 767–814 (1992)
81. E.W. Seely, C.G. Solomon, Insulin resistance and its potential role in pregnancy-induced hypertension. J. Clin. Endocrinol. Metab. **88**, 2393–2398 (2003)

82. M. Straume, S.G. Frasier-Cadoret, M.L. Johnson, Least-squares analysis of fluorescence data, in *Topics in Fluorescence Spectroscopy,* ed. by J.R. Lakowicz, (Plenum Press, New York, 1991), pp. 177–240
83. C. Stringari, J.L. Nourse, L.A. Flanagan, E. Gratton, Phasor fluorescence lifetime microscopy of free and protein-bound NADH reveals neural stem cell differentiation potential. PLoS ONE **7**, e48014 (2012)
84. J. Tan, Cardiovascular disease in pregnancy. Curr. Obstet. Gynaecol. **11**, 137–145 (2001)
85. M. Tanaka, G.K. Mokhtari, R.D. Terry, L.B. Balsam, K.H. Lee, T. Kofidis, P.S. Tsao, R.C. Robbins, Overexpression of human copper/zinc superoxide dismutase (SOD1) suppresses ischemia-reperfusion injury and subsequent development of graft coronary artery disease in murine cardiac grafts. Circulation **110**, II200–II206 (2004)
86. M. Tanaka, S. Nakae, R.D. Terry, G.K. Mokhtari, F. Gunawan, L.B. Balsam, H. Kaneda, T. Kofidis, P.S. Tsao, R.C. Robbins, Cardiomyocyte-specific Bcl-2 overexpression attenuates ischemia-reperfusion injury, immune response during acute rejection, and graft coronary artery disease. Blood **104**, 3789–3796 (2004)
87. G. Vassalli, A. Gallino, M. Weis, W. von Scheidt, L. Kappenberger, L.K. von Segesser, J.J. Goy, Alloimmunity and nonimmunologic risk factors in cardiac allograft vasculopathy. Eur. Heart J. **24**, 1180–1188 (2003)
88. P.J. Verveer, A. Squire, P.I. Bastiaens, Global analysis of fluorescence lifetime imaging microscopy data. Biophys. J. **78**, 2127–2137 (2000)
89. M. Wakita, G. Nishimura, M. Tamura, Some characteristics of the fluorescence lifetime of reduced pyridine nucleotides in isolated mitochondria, isolated hepatocytes, and perfused rat liver in situ. J. Biochem. (Tokyo) **118**, 1151–1160 (1995)
90. R.L. White, B.A. Wittenberg, NADH fluorescence of isolated ventricular myocytes: effects of pacing, myoglobin, and oxygen supply. Biophys. J. **65**, 196–204 (1993)
91. R.L. White, B.A. Wittenberg, Mitochondrial NAD(P)H, ADP, oxidative phosphorylation, and contraction in isolated heart cells. Am. J. Physiol. Heart Circ. Physiol. **279**, H1849–H1857 (2000)
92. M. Wolf, C.A. Hubel, C. Lam, M. Sampson, J.L. Ecker, R.B. Ness, A. Rajakumar, A. Daftary, A.S. Shakir, E.W. Seely, J.M. Roberts, V.P. Sukhatme, S.A. Karumanchi, R. Thadhani, Preeclampsia and future cardiovascular disease: potential role of altered angiogenesis and insulin resistance. J. Clin. Endocrinol. Metab. **89**, 6239–6243 (2004)
93. Z. Xie, T. Cai, Na+-K+-ATPase-mediated signal transduction: from protein interaction to cellular function. Mol. Interv. **3**, 157–168 (2003)
94. Z. Xie, P. Kometiani, J. Liu, J. Li, J.I. Shapiro, A. Askari, Intracellular reactive oxygen species mediate the linkage of Na+/K+-ATPase to hypertrophy and its marker genes in cardiac myocytes. J. Biol. Chem. **274**, 19323–19328 (1999)
95. M.H. Yamani, S.W. van de Poll, N.B. Ratliff, B.E. Kuban, R.C. Starling, P.M. McCarthy, J.B. Young, Fluorescence spectroscopy of endomyocardial tissue post-human heart transplantation: does it correlate with histopathology? J. Heart Lung Transplant. **19**, 1077–1080 (2000)
96. J.H. Yang, E.S. Yang, J.W. Park, Inactivation of NADP + -dependent isocitrate dehydrogenase by lipid peroxidation products. Free Radic. Res. **38**, 241–249 (2004)
97. T. Zimmermann, J. Rietdorf, R. Pepperkok, Spectral imaging and its applications in live cell microscopy. FEBS Lett. **546**, 87–92 (2003)